A template-free electrochemical deposition route to ZnO nanoneedle arrays and their optical and field emission properties



2005 Nanotechnology 16 2567

(http://iopscience.iop.org/0957-4484/16/11/017)

INSTITUTE OF PHYSICS PUBLISHING NANOTECHNOLOGY
Nanotechnology **16** (2005) 2567–2574 doi:10.1088/0957-4484/16/11/017

# A template-free electrochemical deposition route to ZnO nanoneedle arrays and their optical and field emission properties

**Bingqiang Cao[1,2], Weiping Cai[1,4], Guotao Duan[1], Yue Li[1], Qing Zhao[3] and Dapeng Yu[3]**

[1] Key Laboratory of Materials Physics, Anhui Key Laboratory of Nanomaterials and Nanostructures, Institute of Solid State Physics, Chinese Academy of Sciences, Hefei, 230031, Anhui, People's Republic of China
[2] The Graduate School of Chinese Academy of Sciences, Beijing 100039, People's Republic of China
[3] Electron Microscopy Laboratory, Peking University, Beijing 100871, People's Republic of China

E-mail: wpcai@issp.ac.cn

Received 14 July 2005, in final form 23 August 2005
Published 13 September 2005
Online at stacks.iop.org/Nano/16/2567

**Abstract**
We report a soft and template-free electrochemical deposition method for preparing wafer-scale ZnO nanoneedle arrays on an oriented gold film coated silicon substrate. It has been shown that the ZnO nanoneedles possess single-crystal wurtzite structure and grow along the *c*-axis perpendicularly on the substrate. Raman and resonant Raman scattering studies have confirmed that the ZnO nanoneedles are of good crystal quality. The room temperature photoluminescence spectrum of such ZnO nanoneedle arrays exhibits a strong ultraviolet emission but negligible visible emission. The time-resolved photoluminescence spectral analysis discloses the excitonic origin of the ultraviolet emission. The field electron emission study, showing notable emission current in a moderate turn-on field, demonstrates potential applications of such ZnO nanoneedle arrays in field emission display devices. The formation of such a ZnO nanoneedle array is attributed to the formation of {0001}-oriented ZnO nuclei on the oriented gold coated silicon substrate and preferential growth along ⟨0001⟩.

(Some figures in this article are in colour only in the electronic version)

## 1. Introduction

One-dimensional (1D) nanostructures, such as semiconductor nanowires, nanobelts and nanotubes, could be ideal building blocks for the assembly of nanoelectronics and nanophotonics systems because they can function both as nanoscale devices and as the links that access them [1]. Zinc oxide (ZnO), a II–VI compound semiconductor with a direct band gap of 3.37 eV and a relatively high exciton binding energy (60 meV) at room temperature, displays excellent piezoelectric, catalysis and novel optical properties [2]. Although many 1D ZnO nanostructures have been synthesized by various methods [3], it must be acknowledged that these need to be integrated or to be arrayed in three dimensions to find their practical applications in nanodevices. Since the demonstration of room temperature lasing actions of the highly oriented and ordered ZnO nanowire arrays [4], many methods have been developed for obtaining ZnO nanowire arrays. The most direct route for preparing nanowire arrays is the template-assisted method that

[4] Author to whom any correspondence should be addressed.

fills the straight nanochannels of anodic aluminium membrane by the electrochemical deposition (ECD) method [5a], sol–gel method [5b] or vapour deposition method [5c, 5d]. But the ordered arrays will be destroyed when the template is removed. Another very popular strategy is a vapour phase method; examples include the (metal-catalysed) thermal vapour transport and sedimentation method [6], pulsed laser deposition (PLD) method [7] and hydrogen-treated ZnO film method [8]. In addition, Yang *et al* and Vayssieres [9] have developed seed-induced hydrothermal methods for preparing ZnO nanowire arrays on silicon or glass substrates in an autoclave.

As a special nanowire array type, ZnO nanoneedle arrays, because of their tips showing a sharp curvature, are expected to be of particular importance in field emission, besides having novel optical properties. ZnO nanoneedle arrays have been prepared by a vapour phase method on silicon or gallium-doped ZnO film substrate [10]. The vapour phase methods need high preparation temperatures and energy-consuming experimental facilities, and are of low productivity. In contrast, solution approaches are attractive due to their low cost and potential for scaling up. So preparation of ZnO nanoneedle arrays by a soft solution method at a low cost is still appealing in view of the potential applications in nanodevices. The method of ECD from dissolved aqueous precursors is a low cost and scalable method that is usually well suited to mass production of semiconductor thin films. The preparation of ZnO films and their UV light emission properties have been demonstrated [11]. In this paper, we report a template-free ECD method for preparing highly ordered ZnO nanoneedle arrays on an oriented gold film coated silicon (Au/Si) substrate. Such fabrication was conducted at a lower temperature (∼70 °C) and at atmospheric pressure. Detailed Raman scattering spectral studies have indicated that the ZnO nanoneedle arrays are of high crystal quality. Such ZnO nanoneedle arrays exhibited strong ultraviolet excitonic emission and efficient field emission properties, which indicate potential applications in future photoelectric and flat display devices at low industrial costs.

## 2. Experiment

Au/Si substrates were prepared by thermal evaporation of gold at a vacuum of $1 \times 10^{-5}$ Pa. The gold deposition rate was about 0.5 Å $min^{-1}$, controlled by a film thickness monitor (FTM-V, Shanghai). A gold layer about 50 nm thick was deposited on doped single-crystal silicon (100) with low resistivity, smaller than 10 Ω cm. Galvanostatic cathodic deposition on an Au/Si substrate at a current of 0.9 mA was employed. Zinc sheets (99.99% purity) acted as the anode and the electrolyte was zinc nitrate aqueous solution (0.05 M). The pH value of the solution was about 6. The deposition temperature was fixed at 355 K by a water bath and the deposition time was 2 h.

The samples were characterized using a field emission scanning electron microscope (FE-SEM, FEI, Sirion 200), x-ray diffraction (XRD, Philips X'Pert, Cu K$\alpha$ line: 0.154 19 nm) and a transmission electron microscope (TEM, JEOL-2010). Raman and photoluminescence (PL) spectra were recorded using a LABRAM-HR Micro-Raman spectrometer (Jobin-Yvon) excited with the 514.5 nm $Ar^+$ laser or a 325 nm He–Cd laser. The time-resolved photoluminescence (TRPL) spectrum was measured using a FLS920 (EDINBURGH) fluorescence spectrophotometer excited with a nanosecond flash lamp. The field emission measurements were performed in a vacuum chamber at a pressure of $5 \times 10^{-7}$ Pa at room temperature in a two-parallel-plate configuration. The sample or ZnO array, with an area of about 0.1 $cm^2$, on the Au/Si substrate, was attached to a stainless-steel plate using conducting glue as the cathode with the other as the anode. The sample was first heated for 30 min by applying a 3 kV voltage to degas and to further improve the vacuum. The distances between the electrodes were 100, 150, 200 $\mu$m. A voltage with a sweep step of 50 V was applied between the anode and cathode to supply an electric field. The applied voltage was increased from 1 to 5 kV. The emission current was monitored with a Keithley 485 picoammeter.

## 3. Results and discussion

### 3.1. Characterization

Figures 1(a) and (b) show the morphology of the as-synthesized sample on an Au/Si substrate prepared by the ECD method. We can see that the products consist of straight nanowires or nanorods with needle-like tips, which we call nanoneedles, and exhibit a well-aligned array on the substrate surface, perpendicularly. The XRD has confirmed that such nanoneedles are ZnO with wurtzite structure (see the following). Figure 1(c) is the TEM image of a single ZnO nanoneedle gently transferred onto a copper grid by ultrasonication. Typically, the nanoneedles, electrodeposited in 0.05 M $Zn(NO_3)_2$ precursor solution for 2 h, exhibit mean lengths of about two micrometres with tips of tens of nanometres in curvature radius. High-resolution TEM examination has indicated that the whole ZnO nanoneedle is of a single-crystal structure without visible defects, as typically illustrated in figure 1(d), which clearly shows the (0001) crystal planes perpendicular to the axis of the nanoneedle, indicating that ⟨0001⟩ is the preferred growth direction of these wurtzite ZnO nanoneedles and perpendicular to the substrate. The corresponding selected area electron diffraction further proves the single-crystal nature of the nanoneedles and their ⟨0001⟩ growth direction (see the inset of figure 1(d)).

Figure 2 shows the corresponding XRD pattern of the ZnO nanoneedle array on the substrate. There are only two peaks: a very strong peak and a very weak peak from ZnO(002) and ZnO(004), respectively, in addition to the other two weak peaks of Au(111) and Si(400) from the oriented Au/Si substrate. This means that the ZnO nanoneedle array is highly preferentially oriented along the *c*-axis, which is in accordance with the SEM observations. Meanwhile, an XRD $\theta$ rocking curve was also measured to study the degree of alignment with the normal direction of the substrate surface. The rocking curve of the ZnO(002) peak is illustrated in the inset of figure 2. The full width at half-maximum (FWHM) of the curve is 7.5°, which is similar to that of the ZnO nanowire arrays grown on silicon or undoped ZnO film substrates by the vapour phase epitaxy method [6c, 10a].

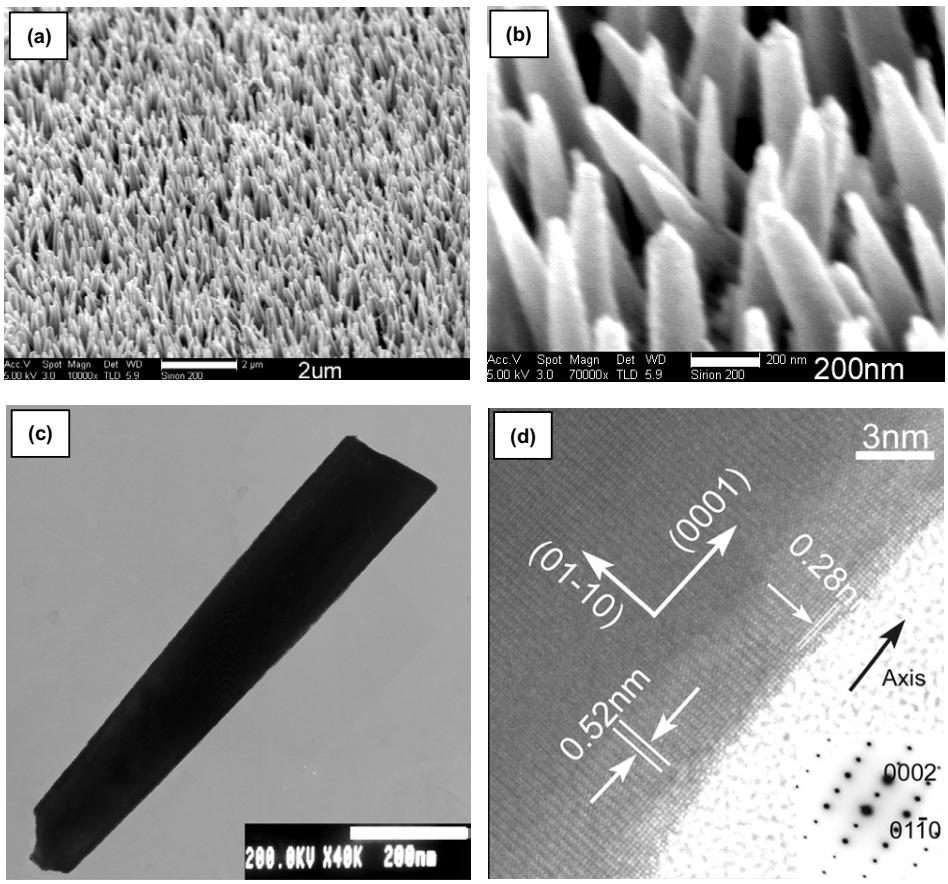


**Figure 1.** (a) FESEM images of an as-prepared sample on the Au/Si substrate and (b) a magnified view of (a); (c) TEM image of a single nanoneedle; (d) HRTEM image of a nanoneedle and its corresponding selected area electron diffraction pattern (inset).

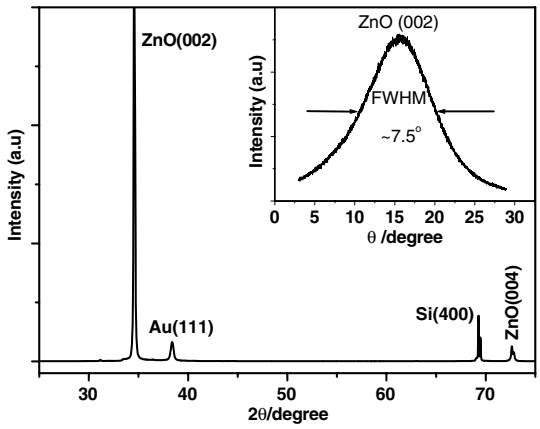


**Figure 2.** XRD pattern of the as-prepared sample on the Au/Si substrate; inset: $\theta$ rocking curve of the ZnO(002) peak with a FWHM of 7.5°.

### *3.2. Raman scattering*

Due to the sensitivity to the crystallization, structural disorder and defects in the nanostructures, Raman scattering was recorded to investigate the crystal quality and vibration properties of the ZnO nanoneedles. Wurtzite ZnO crystal has two formula units per primitive cell and belongs to the $C_{6v}^4$ space group. According to the group theory analysis, the $A_1 + E_1 + 2E_2$ modes are Raman active [12]. Moreover, the $A_1$ and $E_1$ modes are polar and hence split into LO and TO components. In our experiment, the incident laser light was parallel to the ZnO nanoneedles and the Raman signal was recorded in the backscattering geometry. According to the Raman selection rules [13], LO and $E_2$ modes are allowed, while the TO modes of $A_1$ (379 $cm^{-1}$) and $E_1$ (407 $cm^{-1}$) are forbidden. Figure 3(a) shows the Raman spectrum of the ZnO nanoneedle array on the Au/Si substrate excited by a 514.5 nm $Ar^+$ laser, where the strong and characteristic $E_2$ (high) mode at 437 $cm^{-1}$, in addition to the weak $A_1$(LO) mode at 573 $cm^{-1}$ and second-order $^2E_2$ mode at 332 $cm^{-1}$, can be seen. The peak at 520 $cm^{-1}$ is the Raman signal from the silicon substrate because of the penetration of the excitation laser light. The peak position of the $E_2$ mode was red shifted by about 3 $cm^{-1}$ compared with that for bulk ZnO powders [6b]. This red shift is attributed to the optical phonon confinement effect in nanostructures that can cause uncertainty in the phonon wavevectors and a downshift of the Raman peaks [14].

As we know, ZnO has a direct band gap of 3.37 eV and a large polaron coupling coefficient [15]. Therefore, if we use the exciting photon energy in the proximity of the electronic interband transition energy, the polar symmetry LO modes will be dominant, since the resonance enhancement of LO phonons is much stronger than that of the TO modes and other non-polar phonons, such as $E_2$. That is, multiphonon resonant

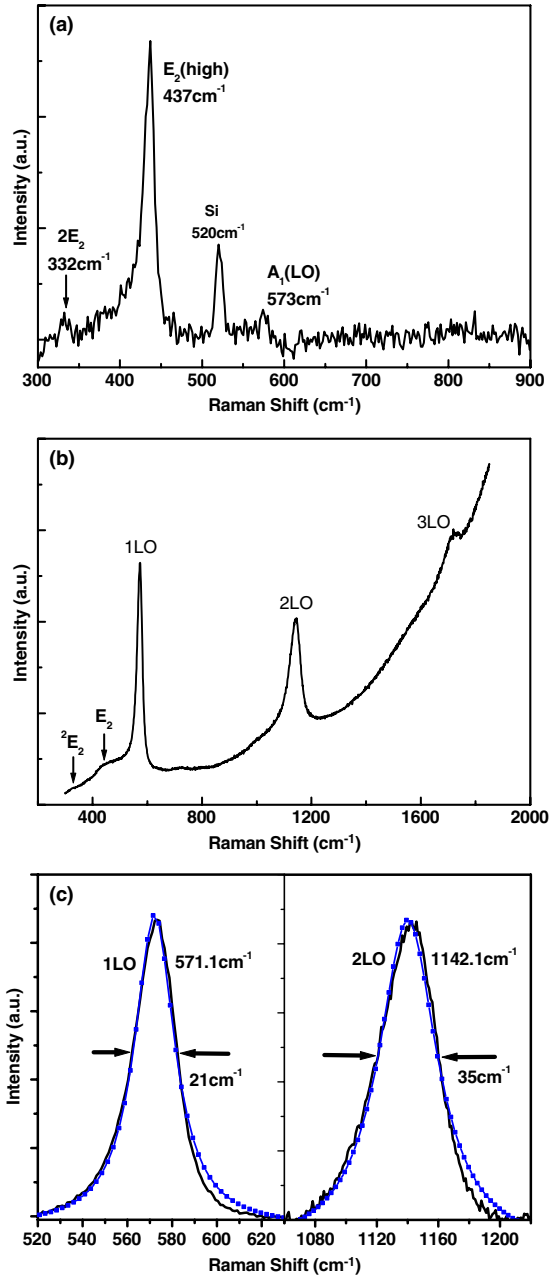


**Figure 3.** Raman spectra of the ZnO nanoneedle array on the Au/Si substrate excited by (a) a 514.5 nm $Ar^+$ laser and (b) a 325 nm He–Cd laser; (c) Lorentzian fitting profile of the 1LO and 2LO peaks in (b).

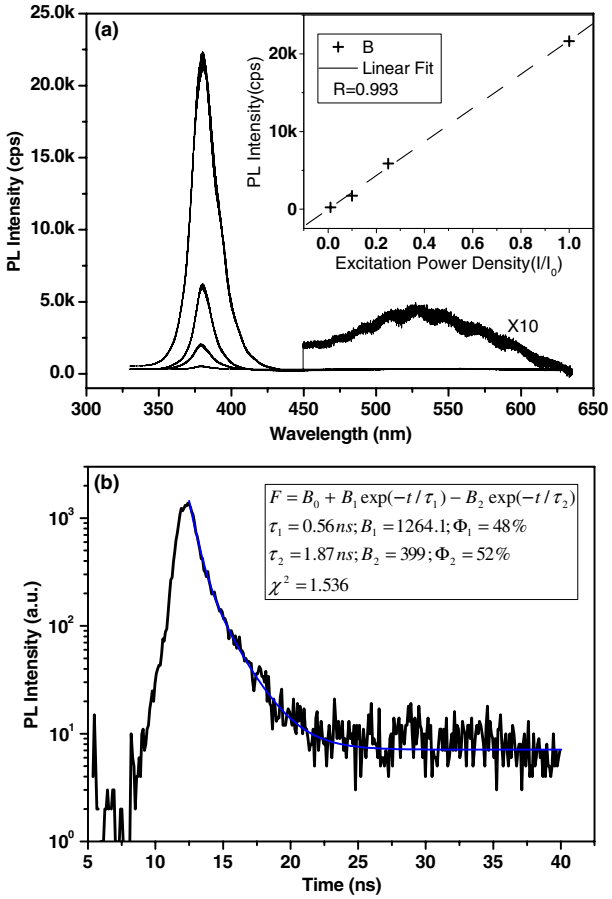


**Figure 4.** (a) Room temperature PL spectra of the ZnO nanoneedle array excited by a 325 nm He–Cd laser at different excitation power intensities; the curves from bottom to top correspond to the excited intensities $0.01I_0$, $0.1I_0$, $0.25I_0$ and $1.00I_0$; inset of (a): integrated PL intensity versus excited power intensity; magnified part: 10× the (450–550 nm) region of the top PL spectrum; (b) TRPL spectrum of the ZnO nanoneedle array monitored at 380 nm, excited by 325 nm light with a nanosecond flash lamp; inset: biexponential fitting results; $\chi^2$: reduced chi squared value; Φ: relative fluorescence intensities.

Raman scattering (MRRS) processes will happen. Figure 3(b) is the corresponding Raman spectrum of the ZnO nanoneedle array, excited with a 325 nm (3.82 eV) He–Cd laser. We can see three major peaks, centred at 571, 1142 and 1723 $cm^{-1}$, superimposed upon the PL background, in addition to the almost imperceptible $E_2$ and $^2E_2$ modes. These sharp lines are at multiples of the frequency of 571 $cm^{-1}$ and can be attributed to the Raman 1LO mode and its overtones [16]. Due to the anisotropic short-range force in the uniaxial ZnO lattice, the 1LO mode usually consists of contributions from both $A_1$(LO) and $E_1$(LO) (9 $cm^{-1}$ in the frequency interval between them) [15]. However, Lorentzian curve fitting has revealed that the 1LO and 2LO peaks in figure 3(b) consist mostly of the $A_1$(LO) mode and the contribution from the $E_1$(LO) is negligible, as illustrated in figure 3(C), since the $E_1$(LO) mode is ascribable to the defects in ZnO, such as oxygen vacancies and zinc interstitials [17]. The absence of the $E_1$(LO) mode indicates the good crystal quality of the nanoneedles. Moreover, the linewidths of the 1LO and 2LO modes are 21 and 35 $cm^{-1}$, respectively, which are much broader than the results predicted by the formula $\Delta\lambda^{-1}$ $(j\text{LO}) = 9j$ $cm^{-1}$, where $\Delta\lambda^{-1}$ is the FWHM of the $j$th-order LO mode [16], and the resonant Raman peaks also show obvious asymmetry. These facts are further evidence of the optical phonon confinement effect in nanostructures [14].

### *3.3. PL and TRPL spectra*

The optical properties of the ZnO nanoneedle arrays at room temperature were studied using a PL spectrum excited with a 325 nm He–Cd laser. Figure 4(a) shows the PL spectra detected under the same conditions but excited with different

laser power densities. The full laser excitation power intensity ($I_0$) is about 2 kW cm$^{-2}$. A dominant emission peak centred at about 380 nm (3.26 eV), near the band edge, was observed for all spectra. With increases of excitation power density, the integrated intensity of the UV PL peak increases linearly, as shown in the inset of figure 4, but the UV peak does not show any detectable shift. These findings indicate that the sharp PL peak originates from the recombination of free or bound excitons [18]. Furthermore, the FWHM of the excitonic emissions are estimated to be 110 meV, smaller than the value for ZnO nanowire arrays (120 meV) grown on anodic aluminium or silicon substrate by the CVD method [5d, 6b] and the same as that for ZnO nanowires grown on *m*-sapphire substrates by the carbothermal method [16]. This narrow FWHM proves the high crystal quality of the ZnO nanoneedles and their narrow size distribution. Commonly, there is another emission peak centred around at 520 nm in the ZnO room temperature PL spectrum, in addition to the UV emission peak, which is generally attributed to the deep-level defects in ZnO crystals, such as vacancies and interstitials of zinc or oxygen [19]. In this work, the green emission is so weak that it can be neglected (see figure 4). The strong and sharp UV emission and the weak green emission also indicate that the ZnO nanoneedle arrays prepared by the ECD method are of good crystal quality.

Further, a room temperature time-resolved PL (TRPL) spectrum was measured in an effort to understand the radiative recombination mechanism of the UV emission. Figure 4(b) shows the TRPL of the UV emission monitored at 380 nm, excited by a nanosecond flash lamp. The decaying region of the TRPL spectrum can be well fitted by a biexponential decay function:

$$F = B_0 + B_1 \exp(-t/\tau_1) + B_2 \exp(-t/\tau_2), \qquad (1)$$

where $F$ is the intensity, $\tau_1$, $\tau_2$ and $B_1$, $B_2$ are the decay time constants (lifetime) and their relative amplitudes, respectively. $B_0$ is the fitting constant. The values of the different parameters, obtained by least-squares fitting, are also shown in figure 4(b). The fast/slow decay time constants and their relative contributions to the fluorescence intensities are 0.56 ns (48%) and 1.87 ns (52%), respectively. This biexponential behaviour strongly suggests that two different decay or capture processes, which are comparable in intensity, are involved in the UV emission. The short decay time constant probably represents the free exciton recombination at room temperature, which is similar to the reported lifetime (0.585 ns) of free excitons in single-crystal ZnO [20]. An increase in the radiative lifetime is theoretically expected for localized excitons in semiconductors [21]. The long decay time constant (1.87 ns) is comparable to the radiative lifetime ($\tau_R$) of electrons in excited states predicted by the formula [22]

$$\tau_R = 2\pi m_0 \varepsilon_0 c^3 / n^2 e^2 \omega^2 f, \qquad (2)$$

where $n$ is the refractive index, $m_0$, $\varepsilon_0$, $c$, $\omega$ and $e$ are the fundamental physical constants with their usual meanings and $f$ is the oscillator strength with a value of about 1 as its upper limit for bound excitons. By using $\omega = 4.95 \times 10^{15}$ s$^{-1}$ and $n = 2.4$ for ZnO [23], $\tau_R$ is estimated to be slightly over 1 ns. So the long decay time constant could be attributed to the radiative lifetime for the excitons bound to the surface or band tail states, which is similar to that reported for the ZnO film grown on a sapphire substrate [24]. The TRPL results also demonstrate the excitonic origin of the UV emissions.

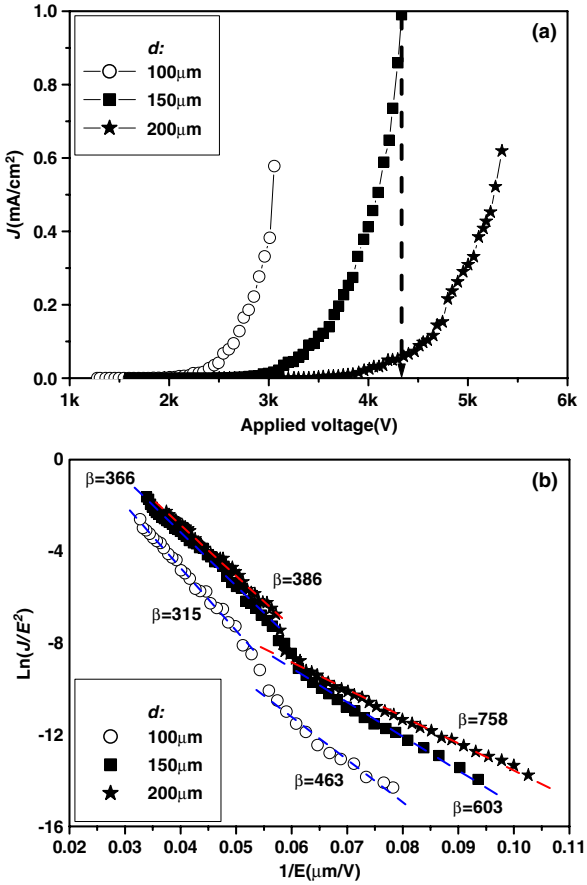


**Figure 5.** (a) Field emission curves of the ZnO nanoneedle array measured for different distances between the anode and cathode; (b) FN plots corresponding to (a).

### 3.4. Field emission

The field emission properties of these nanoneedle arrays were measured in a vacuum chamber at room temperature in a two-parallel-plate configuration. Figure 5(a) shows the current density versus applied voltage ($J$–$V$) curves for the ZnO nanoneedle array for various distances ($d$) between the electrodes. The turn-on field, defined as the applied field needed to draw an emission current of 10 $\mu$A cm$^{-2}$, is about 22.1, 19.3 and 18.9 V $\mu$m$^{-1}$, corresponding to the $d$ values 100, 150, 200 $\mu$m, respectively, lower than the turn-on value (18 V $\mu$m$^{-1}$ for 0.01 $\mu$A cm$^{-2}$) for ZnO needles grown on gallium-doped ZnO film by the vapour phase method [10c]. Our value is comparable to that for the silicon nanocone arrays prepared by ion sputtering [25]. A current density as high as 1 mA cm$^{-2}$ corresponds to the applied voltage of 4.3 kV (figure 5(a)) when $d = 150$ $\mu$m, which is also comparable to those of other wide band gap semiconductors, such as GaN nanowire [26a] and AlN nanocone [26b] arrays on silicon substrates.

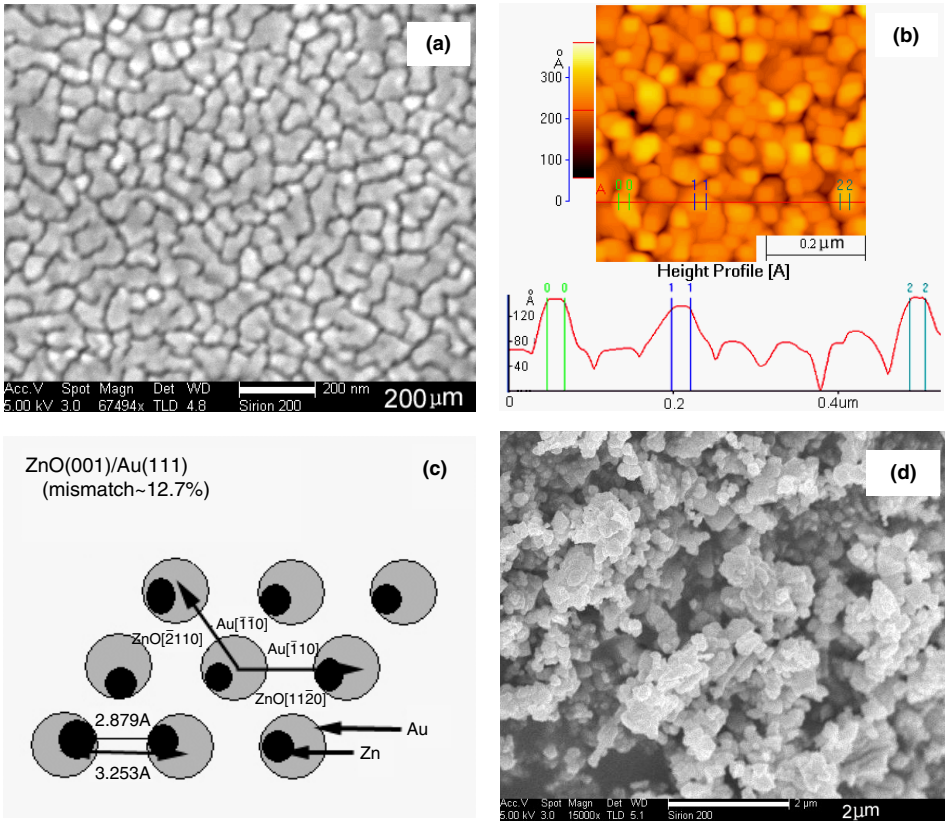


**Figure 6.** ((a), (b)) FESEM and AFM images, and the height profile of the Au/Si substrate surface; (c) the scheme of the orientation relationship of ZnO(0001)/Au(111); (d) ZnO film on the Si substrate electrodeposited with the same parameters as for figure 1(a).

According to the Fowler–Nordheim (FN) theory, the relationship between the current density ($J$) and applied electric field ($E$) can be described as follows [27]:

$$J = A\left(\frac{\beta^2 E^2}{\Phi}\right)\exp\left(\frac{-B\Phi^{3/2}}{\beta E}\right), \qquad (3)$$

where $A = 1.54 \times 10^{-10}$ (A V$^{-2}$ eV), $B = 6.83 \times 10^9$ (V m$^{-1}$ eV$^{-3/2}$) and $\Phi$ is the work function, which is about 5.4 eV for ZnO [10b]. Also $\beta$ is the field enhancement factor, defined as $E_{\text{local}} = \beta E = \beta V/d$, where $E_{\text{local}}$ is the local electric field near to the emitter tip. According to equation (3), the plot of $\ln(J/E^2)$ versus $E^{-1}$ (the FN plot) should be a straight line. Using data in figure 5(a), corresponding FN plots for different $d$ values are shown in figure 5(b). All the FN plots show nearly straight lines with slightly different slopes, indicating that the process of field emission from the ZnO nanoneedle arrays is a barrier tunnelling, quantum mechanical process (FN mechanism) [28]. The observed kinks in the FN plots, which are located in the turn-on field region, can be attributed to the current-induced changes in the structures of the field emitters [29a] or absorbate-induced emission saturation [29b]. The slopes obtained from the FN plots can be used to estimate the $\beta$ values, as shown in figure 5(b), which are comparable to the values for ZnO nanotips [30a] (657 at $d = 250$ $\mu$m) and multiwall carbon nanotubes [30b] (830 at $d = 125$ $\mu$m). Such well-aligned ZnO nanoneedle arrays, with low preparation cost and wafer scale, could hold promise for industrial application of flat displays in the near future.

### *3.5. Growth mechanism*

Now let us discuss the mechanism of growth of the ZnO nanoneedle arrays on the oriented gold film coated silicon substrate. From the chemical reaction point of view, the one-step electrochemical deposition used to prepare the ZnO film has been proposed in previous reports [11a], which mainly make use of the reduction effect of $NO_3^-$ ions at a slightly high temperature (70 °C). As for the ZnO nanoneedle array growth mechanism, first, we should consider the ZnO crystal structure itself. It is well known that ZnO is a kind of polar crystal and the polar plane {0001} has higher surface energy than the other two non-polar surfaces, $\{2\bar{1}\bar{1}0\}$ and $\{01\bar{1}0\}$. So fast crystal growth along the ⟨0001⟩ direction is energetically favourable under thermodynamical equilibrium conditions [2]. On the other hand, the working electrode should also have an important influence on the ZnO crystal nucleation and growth process in an ECD experiment.

The FESEM and atom force microscopy (AFM) observations of the Au/Si electrode are shown in figures 6(a), (b). It can be seen that the gold film is composed of smooth and featureless islands with about 100 nm size. XRD measurement indicates that such gold film has a strong preferential orientation of Au(111) planes parallel to the Si substrate (figure 2). In the initial period of the ECD process, ZnO will nucleate on the flat gold island on the cathode surface. Since the interface energy is directly related to the lattice mismatch of interfaces [31], to lower the interface energy there will need to be an orientation relationship between the ZnO nuclei and the Au film to reduce

the lattice mismatch between them, which can be deduced to be $(1 \times 1)$ZnO$(0001)[11\bar{2}0] \parallel (1 \times 1)$Au$(111)[\bar{1}10]$ [32]. Figure 6(c) shows schematically such a relationship, which results in the smallest lattice mismatch in the interface between ZnO$\{0001\}$ and gold$\{111\}$, with a lattice mismatch along ZnO$\langle 11\bar{2}0\rangle$ and Au$\langle\bar{1}10\rangle$ of 12.7%. These $\{0001\}$-oriented ZnO nuclei will serve as seeds and grow preferentially along the *c*-axis, which happens to be perpendicular to the substrate, due to the high surface free energy of polar $\{0001\}$ crystal planes [33], and the growth rates along $[10\bar{1}1]$ and $[01\bar{1}0]$ directions are slower in turn [34]. Finally, the needle-like ZnO nanoneedle arrays were developed due to the effect of proximity of the nanoneedles [6b].

Obviously, the $\{111\}$-oriented Au film is absolutely necessary for forming the ZnO nanoneedle array. It is this $\{111\}$-oriented Au film that leads to the formation of $\{0001\}$-oriented ZnO nuclei, which grow preferentially along the *c*-axis, and hence the oriented nanoneedle array. This means that a ZnO nanoneedle array will not be formed on the substrate without the $\{111\}$-oriented Au film. Further experiment has confirmed that ECD on the silicon substrate without an Au coating only induces a ZnO film consisting of randomly oriented nanoparticles, as shown in figure 6(d).

## 4. Conclusions

In summary, we reported a soft and template-free electrochemical deposition method for preparing ZnO nanoneedle arrays. The $\{111\}$-oriented Au film/Si substrate results in the formation of $\{0001\}$-oriented ZnO nuclei on the film due to the small lattice mismatch between them. The oriented ZnO nuclei serve as seeds and grow preferentially along the *c*-axis due to the high surface free energy of the $\{0001\}$ polar plane, leading to the formation of the ZnO nanoneedle array perpendicular to the substrate. This ZnO nanoneedle array is of good crystal quality and hence exhibits strong UV emission but very weak visible PL. It also shows efficient field emission comparable to that of other semiconductor nanoneedle arrays prepared by the vapour phase method, which demonstrates the potential for applications in future photoelectric and flat display devices, at low industrial costs.

## Acknowledgments

The authors acknowledge the financial support from the National Natural Science Foundation of China (Grant numbers: 50271069 and 10474099) and the National Project for Basic Research (Grant No 2006CB300402)

## References

[1] Hu J T, Odom T W and Lieber C M 1999 *Acc. Chem. Res.* **32** 435
[2a] See review: Wang Z L 2004 *J. Phys.: Condens. Matter* **303** R829
[2b] Wang Z L, Kong X Y, Ding Y, Gao P X, Hughes W L, Yang R S and Zhang Y 2004 *Adv. Funct. Mater.* **14** 943
[3a] Pan Z W, Dai Z R and Wang Z L 2001 *Science* **291** 1947
[3b] Gao P X, Ding Y and Wang Z L 2003 *Nano Lett.* **9** 1315
[3c] Wang Z L, Kong X Y and Zou J M 2003 *Phys. Rev. Lett.* **91** 185502
[3d] Hu J Q, Li Q, Meng X M, Lee C S and Lee S T 2003 *Chem. Mater.* **15** 305
[3e] Yang R S, Ding Y and Wang Z L 2004 *Nano Lett.* **4** 1309
[4] Huang M H, Mao S, Feick H, Yan H Q, Wu Y Y, Kind H, Weber E, Russo R and Yang P D 2002 *Science* **292** 1897
[5a] Li Y, Meng G W, Zhang L D and Phillip F 2002 *Appl. Phys. Lett.* **76** 2011
[5b] Wu G S, Zhang L D, Cheng B C, Xie T and Yuan X Y 2004 *J. Am. Chem. Soc.* **126** 5976
[5c] Liu C H, Zapien J A, Yao Y, Meng X M, Lee C S, Fan S S, Lifshitz Y and Lee S T 2003 *Adv. Mater.* **15** 838
[5d] Jie J S, Wang G Z, Wang Q T, Chen Y M, Han X H, Wang X P and Hou J G 2004 *J. Phys. Chem.* B **108** 11976
[6a] Wang X D, Summers C J and Wang Z L 2004 *Nano Lett.* **4** 423
[6b] Geng C Y, Jiang Y, Yao Y, Meng X M, Zapien J A, Lee C S, Lifshitz Y and Lee S T 2004 *Adv. Funct. Mater.* **14** 589
[6c] Jie J S, Wang G Z, Chen Y M, Han X H, Wang Q T, Xu B and Hou J G 2005 *Appl. Phys. Lett.* **86** 031909
[7a] Choi J H, Tabata H and Kawai T 2001 *J. Cryst. Growth* **226** 493
[7b] Lorenz M, Kaidashev E M, Rahm A, Nobis Th, Lenzner J, Wagner G, Spemann D, Hochmuth H and Grundmann M 2005 *Appl. Phys. Lett.* **86** 143113
[8] Wu J J, Wen H I, Tseng C H and Liu S C 2004 *Adv. Funct. Mater.* **14** 806
[9a] Greene L E, Law M, Goldberger J, Kim F, Johnson J C, Zhang Y F, Saykally R J and Yang P D 2003 *Angew. Chem. Int. Edn Engl.* **42** 3031
[9b] Vayssieres L 2003 *Adv. Mater.* **15** 464
[10a] Park W I, Yi G C, Kim M Y and Pennycook S J 2002 *Adv. Mater.* **14** 1841
[10b] Zhu Y W, Zhang H Z, Sun X C, Feng S Q, Xu J, Zhao Q, Xiang B, Wang R M and Yu D P 2003 *Appl. Phys. Lett.* **83** 144
[10c] Tseng Y K, Huang C J, Cheng H M, Lin I N, Liu K S and Chen I C 2003 *Adv. Funct. Mater.* **13** 811
[10d] Fan H J, Scholz R, Dadgar A, Krost A and Zacharias M 2005 *Appl. Phys.* A **80** 457
[11a] Peulon S and Lincot D 1996 *Adv. Mater.* **8** 166
[11b] Izaki M and Omi T 1996 *Appl. Phys. Lett.* **68** 2439
[11c] Wong M H, Berenov A, Qi X, Kappers M J, Barber Z H, Illy B, Lockman Z, Ryan M P and MacManus-Driscoll J L 2003 *Nanotechnology* **14** 968
[11d] Izaki M, Watase S and Takahashi H 2003 *Adv. Mater.* **15** 2000
[12] Arguello C A, Rousseau D L and Porto S P S 1969 *Phys. Rev.* **181** 1351
[13] Zhang Y, Jia H B, Wang R M, Chen C P, Luo X H and Yu D P 2003 *Appl. Phys. Lett.* **83** 4631
[14] Du Y, Zhang M S, Hong J, Shen Y, Chen Q and Yin Z 2003 *Appl. Phys.* A **76** 171
[15] Scoot J F 1970 *Phys. Rev.* B **2** 1209
[16] Ng H T, Chen B, Li J, Han J, Meyyappan M, Wu J, Li S X and Haller E E 2003 *Appl. Phys. Lett.* **82** 2023
[17] Fan H J, Scholz R, Kolb F M, Zacharias M, Gösele U, Heyroth F, Eisenschmidt C, Hempel T and Christen J 2004 *Appl. Phys.* A **79** 1895
[18a] Schmit T, Lischka K and Zulehner W 1992 *Phys. Rev.* B **45** 8989
[18b] Guo B, Qiu Z R and Wong K S 2003 *Appl. Phys. Lett.* **82** 2290
[19] Liu X, Wu X H, Cao H and Chang R P H 2004 *J. Appl. Phys.* **95** 3141
[20] Teke A, Özgür Ü, Doğan S, Gu X, Morkoç H, Nemeth B, Nause J and Everitt H O 2004 *Phys. Rev.* B **70** 195207
[21] Chen G D, Smith M, Lin J Y and Jiang H X 1996 *Appl. Phys. Lett.* **68** 2784
[22] Hooft G W p't, van der Poel W A J A, Molenkamp L W and Foxon C T 1987 *Phys. Rev.* B **35** 8281
[23] Yoshikawa H and Adachi S 1997 *Japan. J. Appl. Phys.* **36** 6237
[24] Jung S W, Park W I, Park H D, Yi G C, Jang H M, Hong S and Joo T 2002 *Appl. Phys. Lett.* **80** 1924

[25] Shang N G, Meng F Y, Au F C K, Li Q, Lee C S, Bello I and Lee S T 2002 *Adv. Mater.* **14** 1308
[26a] Chen C C, Yeh C C, Chen C H, Yu M Y, Liu H L, Wu J J, Chen K H L, Chyong C, Peng J Y and Chen Y F 2001 *J. Am. Chem. Soc.* **123** 2791
[26b] Liu C, Hu Z, Wu Q, Wang X Z, Chen Y, Sang H, Zhu J M, Deng S Z and Xu N S 2005 *J. Am. Chem. Soc.* **127** 1318
[27] Fowler R H and Nordheim L W 1928 *Proc. R. Soc.* A **119** 173
[28] Rinzler A G, Hafner J H, Nikolaev P, Lou L, Kim S G, Tomnek D, Nordlander P, Colbert D T and Ugarte D 1995 *Science* **269** 1550
[29a] Sveningsson M, Morjan E R, Nerushev O A, Sato Y, Bäckström J, Campbell E E B and Rohmund F 2001 *Appl. Phys.* A **73** 409
[29b] Li Y B, Bando Y and Golberg D 2004 *Appl. Phys. Lett.* **84** 3603
[30a] Xu C X and Sun X W 2003 *Appl. Phys. Lett.* **83** 3806
[30b] Bonard J M, Salvetat J P, Stöckli T, Forró L and Châtelain A 1999 *Appl. Phys.* A **69** 245
[31] Verhoeven J D 1975 *Fundamentals of Physical Metallurgy* (New York: Wiley)
[32] Liu R, Vertegel A A, Bohannan E W, Sorenson T A and Switzer J A 2001 *Chem. Mater.* **13** 508
[33a] Choy J H, Jang E S, Won J H, Chung J H, Jang D J and Kim Y W 2003 *Adv. Mater.* **15** 1911
[33b] Fan H J, Bertram F, Dadgar A, Christen J, Krost A and Zacharias M 2004 *Nanotechnology* **15** 1401
[34] Laudise R A and Ballman A A 1960 *J. Phys. Chem.* **64** 688